Struct Multidisc Optim
DOI 10.1007/s00158-012-0868-3

RESEARCH PAPER

On robust design optimization of truss structures with bounded uncertainties

Zhan Kang · Song Bai

Received: 31 March 2012 / Revised: 13 August 2012 / Accepted: 8 September 2012

Abstract This paper investigates robust design optimization of truss structures with uncertain-but-bounded parameters and loads. The variations of the cross-sectional areas, Young's moduli and applied loads are treated with non-probabilistic ellipsoid convex models. A robustness index for quantitatively measuring the maximal allowable magnitude of system variations is presented, and the design problem is then formulated as to maximize the minimum of the robustness indices for all the concerned design requirements under a given material volume constraint. For circumventing the difficulty associated with the max-min type problem, an aggregate function technique is employed to construct a smooth objective function. The computational scheme for the sensitivity of the robustness index is derived on the basis of optimum sensitivity analysis. The optimization problem is then solved by using the GCMMA optimizer. Numerical examples illustrate the validity and effectiveness of the present formulation and solution techniques.

Keywords Structural optimization · Robust design optimization · Uncertainty · Non-probabilistic model · Convex model

1 Introduction

Conventionally, structural optimization is performed under deterministic assumptions. In practical structural design problems, however, system uncertainties are inherent and unavoidable. A structure is usually exposed to uncertainties induced by material property scatter, geometrical dimension imprecision and loading conditions fluctuation, etc. Since these uncertainties may cause significant variability in structural performance, they need to be properly accounted for in the optimal structural design problem (Schueller and Jensen 2008; Beck and de Santana Gomes 2010). Many studies have been devoted to structural optimization against uncertainties arising from various sources, e.g. material properties (Papadrakakis et al. 2005; Asadpoure et al. 2011), geometrical dimensions (Sigmund 2009) and external loads (Pantelides and Ganzerli 1998; Lombardi and Haftka 1998; Ganzerli and Pantelides 2000; Papadrakakis et al. 2005; Kanno and Takewaki 2006; Takezawa et al. 2011). In general, two types of structural optimization formulations have been developed to handle system uncertainties: reliability-based design optimization (RBDO) and robust design optimization (RDO). There are conceptual differences between these two formulations. The former usually treats optimal design problems under given constraints of catastrophic failure probability in rare extreme events, while the latter emphasizes on finding a design that minimizes the response sensitivity with respect to the uncertain variations or allows for the maximum possible system variability in everyday service conditions.

Since Taguchi's (1984) pioneering work on quality control, robust design problems have been addressed in different scientific and engineering fields (e.g. Parkinson 1995; Chen et al. 1996a, b, 2000; Chen and Lewis 1999; Lagaros and Papadrakakis 2007; Lagaros et al. 2010; Zaman et al. 2011; Erfani and Utyuzhnikov 2012). In the context of structural design, most of existing formulations of robust design optimization are based on probabilistic description of the uncertain variations. In particular, the bi-criteria

Z. Kang (✉) · S. Bai
State Key Laboratory of Structural Analysis for Industrial Equipment, Dalian University of Technology, Dalian 116024, China
e-mail: zhankang@dlut.edu.cn

Published online: 03 January 2013

robust design optimization formulation, in which both the expected value and the standard deviation of the goal performance function are to be minimized, has been frequently used. Using this concept, Doltsinis and Kang (2004) explored the application of robust design optimization methods for structures and inelastic deformation processes with the perturbation-based stochastic FE analysis technique (Doltsinis and Kang 2006). Asadpoure et al. (2011) carried out robust topology optimization of truss structures with stiffness uncertainties by applying a numerical strategy that transforms the non-deterministic topology optimization problem into an augmented deterministic one. Lagaros et al. (2005) proposed a non-dominant cascade evolutionary algorithm-based multi-objective optimization method for structural robust design optimization. Sandgren and Cameron (2002) employed a genetic algorithm for seeking robust structural designs by incorporating the standard deviations of the structural responses into the constraints. Chen et al. (2010) and Chen and Chen (2011) studied the robust shape and topology optimization under random loading, material properties and geometrical uncertainties. Guest and Igusa (2008) studied topology optimization of structures with load and nodal position uncertainties described by joint probability density functions. Harzheim and Warnecke (2010), and Sun et al. (2011) performed robust optimization of practical engineering designs using surrogate models. For the details of the robust design optimization models in the probabilistic framework, the interested readers are referred to the survey article by Beyer and Sendhoff (2007) and the references therein.

Probabilistic robust design optimization approaches have been well established. They generally rely on precise data (usually up to second-order moments) of the probability distribution of the random parameters. In some real engineering applications, however, these data might be difficult to be obtained due to lack of sufficient samples. In such circumstances, designers have to make certain assumptions when constructing a probabilistic model. It is pointed out by Elishakoff (1995, 1999) that in some particular cases even small errors in probabilistic data may lead to large errors when estimating the probabilities of failure. Therefore, as appealing supplements to conventional probabilistic models, non-probabilistic uncertainty models, including the convex models (Ben-Haim and Elishakoff 1990; Elseifi et al. 1999; Kang and Luo 2009, 2010; Luo et al. 2009), the interval set (a special instance of convex model) (Jiang et al. 2008; Zhao et al. 2010; Impollonia and Muscolino 2011) and the fuzzy set model (Mourelatos and Zhou 2005; Du et al. 2006) have been considered. Convex models (including the interval set model) provide no information on the occurrence frequency of extreme combination of the uncertainties and thus might be over-conservative in some circumstances. However, one merit of convex models is, only the knowledge of the bounds of the uncertain parameters is required, and the bounds can be obtained on the basis of a small number of samples (Jiang et al. 2007, 2011). The fuzzy set model is capable of describing vague definitions or imprecise mathematical models with certain membership functions (Moller and Beer 2008). These membership functions, however, are to some extent subjective choices.

Among the aforementioned models, the ellipsoid convex model has gained much attention in literature when dealing with bounded uncertainties. In practical engineering design problems, the bounds of the uncertain parameters can be more easily determined as compared to their precise statistical distribution. For example, the bound limits of uncertain geometrical dimensions, which are closely related to the manufacturing error, can be confidently identified from the manufacturing tolerance specifications. The convex models are well suited for describing such kind of unknown-but-bounded parameters. Unlike the probabilistic model relying on precise statistical distribution (particularly the tail distribution), convex models (including the interval sets) can be constructed with relative ease (see e.g. Jiang et al. 2011). Moreover, the mathematically differentiable bound description of ellipsoidal convex models facilitates application of efficient gradient-based optimizer in seeking the extreme function values. Therefore, as an attractive supplement to traditional probabilistic models for describing bounded uncertainties, ellipsoidal convex models have been used in many structural optimization problems involving uncertainties, both in the context of robust design (Ben-Tal and Nemirovski 1997; Yonekura and Kanno 2010) and of reliability-based design (Qiu 2003, 2005; Han et al. 2008; Hu and Qiu 2010; Jiang et al. 2011).

In this work, we first propose a novel robustness measure based on non-probabilistic convex models, which deems a structural design more robust if it can sustain a wider range of uncertain variations. On the basis of the proposed robustness measure, the formulation and numerical techniques for robust design optimization of truss structures are then studied. Therein, the ellipsoid convex model is employed for describing uncertain-but-bounded loads and parameters. The considered problem differs from other existing optimization formulations using ellipsoid convex models in that it aims to maximize the robustness of the structure by allowing for larger parameter variations, rather than to seek an optimal design under prescribed non-probabilistic reliability constraints. The rest of this paper is organized as follows. In Section 2, the non-probabilistic ellipsoid convex modeling techniques are introduced, and a quantified robustness measurement is defined based on the convex model. Section 3 presents the formulation of the optimization problem. In Section 4, the derivative of the proposed robustness index with respect to the design variables is derived and numerical implementations for solving the robust design optimization

problem are discussed. Numerical examples are given in Section 5 and conclusions are drawn in Section 6.

2 Definition of a robustness measure based on convex model

In this section, the basic concept of the ellipsoid convex model for uncertain-but-bounded parameters is first presented. Then, a quantified robustness measure based on the ellipsoid convex model is defined.

2.1 Ellipsoid convex model of uncertainties

Let $\mathbf{y} = \{y_1, y_{2,\ldots,} y_n\}^{\mathrm{T}}$ denotes the uncertain parameter vector that collects all the n uncertain-but-bounded parameters. In order to measure the magnitudes of uncertainties arising from different sources, we define a vector of dimensionless uncertain variables

$$\begin{aligned}\mathbf{z} &= \{z_1, z_2, ..., z_n\}^{\mathrm{T}} \\ &= \left\{ \frac{y_1 - \overline{y}_1}{\overline{y}_1}, \frac{y_2 - \overline{y}_2}{\overline{y}_2}, \ldots, \frac{y_n - \overline{y}_n}{\overline{y}_n} \right\}^{\mathrm{T}},\end{aligned} \tag{1}$$

where $\overline{y}_i$ is the nominal value of the ith uncertain parameter, and by such means the uncertain parameters can be determined by their nominal values and variance about nominal values. In this study, we assume that all the uncertain parameters have non-zero nominal values so that the normalization in (1) can be performed. For those parameters that may take zero nominal values, such as the nodal coordinates, an offset can be applied. The relation in (1) can also be expressed in matrix form as

$$\mathbf{y} = (\mathbf{I} + \mathrm{diag}(\mathbf{z}))\overline{\mathbf{y}}, \tag{2}$$

where $\mathbf{I} \in \Re^{n\times n}$ is an identity matrix, $\mathrm{diag}(\mathbf{z})$ is a diagonal matrix containing the components of the vector $\mathbf{z}$, that is

$$\mathrm{diag}(\mathbf{z}) = \begin{bmatrix} z_1 & 0 & \ldots & 0 \\ 0 & z_2 & & \vdots \\ \vdots & & \ddots & \\ 0 & \ldots & & z_n \end{bmatrix}. \tag{3}$$

Suppose that the reference variations of the uncertainty variables are bounded by an n-dimensional ellipsoid as $\mathbf{Z} = \left\{\mathbf{z} | \mathbf{z}^{\mathrm{T}}\mathbf{W}\mathbf{z} \le 1\right\}$, where $\mathbf{W}$ is a real symmetric positive definite matrix known as the characteristic matrix of the convex model and it defines the principal axes of the ellipsoid. By performing a linear transformation, the dimensionless uncertainty vector $\mathbf{z}$ can be transformed into a normalized space. From geometrical point of view, this transformation transforms the ellipsoid set into a unit-radius hyper-sphere set in the normalized uncertain parameter space. The linear transformation is expressed by

$$\mathbf{z} = \xi\mathbf{T}\boldsymbol{\varphi}, \tag{4a}$$

with

$$\mathbf{T} = \mathbf{Q}\boldsymbol{\Lambda}^{-1/2}, \tag{4b}$$

where ξ is a real scalar, $\mathbf{T}$ is an invertible linear transformation matrix, $\boldsymbol{\varphi}$ is called *the normalized or standardized vector* of the uncertainty vector $\mathbf{z}$, and the normalized space spanned by the vector $\boldsymbol{\varphi}$ is also referred to as $\boldsymbol{\varphi}$-*space*; $\mathbf{Q}$ is an orthogonal matrix consisting of normalized eigenvectors of $\mathbf{W}$ and $\boldsymbol{\Lambda}$ is the diagonal eigenvalue matrix of $\mathbf{W}$. The scalar ξ is used to re-scale the ellipsoid model to define a different range of uncertain variation, particularly $\xi = 1$ corresponds to the prescribed reference variation range.

A point-to-set function (set-valued function) $\mathrm{E}(\xi)$, which is affinely dependent on ξ, is then defined as

$$\mathrm{E}(\xi) = \left\{\mathbf{z} \in \Re^n \,|\mathbf{z} = \xi\mathbf{T}\boldsymbol{\varphi},\ \ \|\boldsymbol{\varphi}\|_2 \le 1, \boldsymbol{\varphi} \in \Re^n\right\}, \tag{5}$$

where the notation $||\cdot||_2$ denotes the Euclidean norm, i.e. $\|\boldsymbol{\varphi}\|_2^2 = \boldsymbol{\varphi}^{\mathrm{T}}\boldsymbol{\varphi}$.

The convex set $\mathrm{E}(\xi)$ can also be expressed in an equivalent form as

$$\mathrm{E}(\xi) = \left\{\mathbf{z} \in \Re^n \,|\mathbf{z} = \mathbf{T}\boldsymbol{\varphi},\ \ \|\boldsymbol{\varphi}\|_2 \le \xi, \boldsymbol{\varphi} \in \Re^n\right\}. \tag{6}$$

In the above expression, $\|\boldsymbol{\varphi}\|_2 \le \xi\ (\boldsymbol{\varphi} \in \Re^n)$ represents a hyper-sphere with a radius ξ in the n-dimensional normalized space.

It is noted that $\mathrm{E}(\xi)$ is a continuous point-to-set mapping function. Moreover, it holds that

$$\mathrm{E}(\xi_1) \subset \mathrm{E}(\xi_2) \ \text{ iff } \xi_1 < \xi_2. \tag{7}$$

2.2 Robustness index

A basic idea in this study is that a structure is termed as more robust if it can withstand larger uncertain system variations. Based on this concept, a quantified robustness measure of structural designs is proposed on the basis of convex modeling, which will be elaborated in what follows.

In a structural design problem, we define the status of a structural performance by a feasibility function $G(\mathbf{x}, \mathbf{z})$ in terms of the design variable vector $\mathbf{x}$ and the uncertainty vector $\mathbf{z}$. This function can also be transformed into normalized $\boldsymbol{\varphi}$-space by the linear transformation defined by (7). We denote by $g(\mathbf{x}, \boldsymbol{\varphi})$ the normalized feasibility function, that is

$$G(\mathbf{x}, \mathbf{z}) = G(\mathbf{x}, \mathbf{z}(\boldsymbol{\varphi})) \triangleq g(\mathbf{x}, \boldsymbol{\varphi}). \tag{8}$$

The normalized uncertainty space is divided into two domains by the feasibility function, namely a feasible domain $\{\boldsymbol{\varphi} \in \Re^n | g(\mathbf{x}, \boldsymbol{\varphi}) > 0\}$ and a non-feasible domain

$\{\boldsymbol{\varphi} \in \Re^n | g(\mathbf{x}, \boldsymbol{\varphi}) < 0\}$, and the critical curve (or critical surface in 3-D cases) is defined by $g(\mathbf{x}, \boldsymbol{\varphi}) = 0$.

For illustrating the definition of the proposed robustness measure, we first consider a simple case with two uncertain variables, as shown in Fig. 1. In the figure, the critical curves corresponding to two given designs $\mathbf{x}_\alpha$ and $\mathbf{x}_\beta$ are depicted in blue and red, respectively, in the normalized uncertainty space. In this 2-D case, the ellipsoid convex models reduce to a set of circles, with their radii reflecting the magnitude of the uncertain variations. Particularly, the dash-line circle with $\xi = 1$ represents the normalized uncertainty model. For a certain design $\mathbf{x}$, one can find a circle that is tangential to the critical curve $g(\mathbf{x}, \boldsymbol{\varphi}) = 0$ by seeking the closest point on the critical curve to the origin of the normalized uncertainty space. For example, the circle tangent to the critical curve for design $\mathbf{x}_\alpha$ is drawn in blue and the tangential points are denoted by point A in Fig. 1. All the combinations of uncertain parameters enclosed in this circle lie in the feasible domain of design $\mathbf{x}_\alpha$. If the circle is further expanded, infeasible combinations of uncertain parameters will be included. Thus, the circle that is tangential to the critical curve represents the maximum allowable variation of the structural system for a fixed design. It is also seen that the radius of the circle (depicted in red) tangential to the critical curve of design $\mathbf{x}_\beta$ is greater than that of design $\mathbf{x}_\alpha$. Therefore, according to the robustness concept aforementioned, design $\mathbf{x}_\beta$ is considered more robust than design $\mathbf{x}_\alpha$.

On the basis of above considerations, we introduce a robustness index for measuring the maximum variability that a structure design $\mathbf{x}$ can sustain. It is expressed by $\xi^* = \left(\boldsymbol{\varphi}^{*\mathrm{T}}\boldsymbol{\varphi}^*\right)^{1/2}$, with $\boldsymbol{\varphi}^*$ being the solution to the following constrained minimization problem:

$$\begin{array}{ll} \text{Find} & \boldsymbol{\varphi} \\ \text{to min.} & \boldsymbol{\varphi}^{\mathrm{T}}\boldsymbol{\varphi}, \\ \text{s.t.} & g(\mathbf{x}, \boldsymbol{\varphi}) \le 0, \end{array} \tag{9}$$

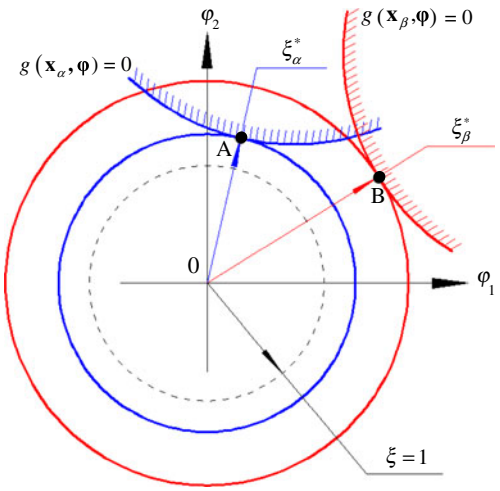

Fig. 1 Illustration of definition of proposed robustness index

where $\boldsymbol{\varphi} \in \Re^n$ is the normalized uncertainty vector. Problem (9) has an explicit quadratic objective function, thus it can be readily treated by a sequential quadratic programming (SQP) algorithm based on linear approximation of the feasibility function.

3 Formulation of robust design optimization problem

In this section, the robust design optimization of truss structures is formulated as a nested optimization problem using the structural robustness measure introduced in Section 2. In the robust design optimization, the robustnesses of several structural performance functions may be simultaneously concerned. To improve the overall robustness of the structural system, the minimum of the robustness indices for all these performance functions is to be maximized, rendering a non-differentiable max-min problem. In order to circumvent the computational difficulty in solving the max-min problem, we apply an aggregate function method to convert the objective function into a smooth one.

3.1 Optimization problem formulation

The considered robust optimization problem is inherently a nested double-level one. The lower-level aims at calculating the robustness indices of specified structural performances, while the upper-level seeks the optimum structural design under a given material volume constraint based on the lower-level solutions. The optimization problem is mathematically stated as

$$\begin{array}{ll} \text{Find} & \mathbf{x} \in \Re^m \\ \text{to max.} & \xi^* \\ \text{s.t.} & \inf\limits_{\boldsymbol{\varphi} \in \mathrm{E}(\xi^*)} g_j(\mathbf{x}, \boldsymbol{\varphi}) \ge 0, \quad j = 1, 2, \ldots, l \\ & V - V^{\mathrm{U}} \le 0, \\ & x_i^{\mathrm{L}} \le x_i \le x_i^{\mathrm{U}}, \quad i = 1, 2, \ldots, m, \end{array} \tag{10}$$

where $\mathbf{x}$ is the vector of design variables, i.e. the sectional areas of the member bars; m is the number of the member bars; x_i^{L} and x_i^{U} are respectively the lower and upper bound for the ith design variable; l is the number of concerned structural performances; $V = \sum\limits_{i=1}^{m} x_i \ell_i$ is the material volume with ℓ_i denoting the bar length, V^U is the upper bound for the material volume.

Problem (10) can be cast into an equivalent double-level formulation as

$$\begin{array}{lll} \text{Upper level:} & \text{Find } \boldsymbol{x} \in \Re^m \\ & \text{to max. } \xi^* = \min\left(\xi_1^*, \xi_2^*, \ldots, \xi_l^*\right) \\ & \text{s.t. } V - V^{\mathrm{U}} \le 0, \\ & \quad x_i^{\mathrm{L}} \le x_i \le x_i^{\mathrm{U}}, \quad i = 1, 2, \ldots, m, \end{array} \tag{11}$$

where m is the number of design variables, $\xi_j^* = \text{sgn}\left(g_j(\mathbf{x}, \mathbf{0})\right) \cdot \left(\boldsymbol{\varphi}_j^{*\mathrm{T}} \boldsymbol{\varphi}_j^*\right)^{1/2}$ is the robust index for the jth behavior function, with sgn$(\cdot)$ being the signum function and $\boldsymbol{\varphi}_j^*$ being the minimizer of the jth lower level constrained minimization problem expressed by

$$\begin{aligned} \text{Lower level } (j\text{th}): \quad & \text{Find} \quad \boldsymbol{\varphi} \in \Re^n \\ & \text{to min.} \quad \boldsymbol{\varphi}^{\mathrm{T}} \boldsymbol{\varphi}, \\ & \text{s.t.} \quad g_j(\mathbf{x}, \boldsymbol{\varphi}) \le 0. \end{aligned} \tag{12}$$

From a geometrical perspective, problem (12) is to seek the hyper-sphere that is tangent to the critical curve in $\boldsymbol{\varphi}$-space under a given constraint.

In above expressions, $\xi_j^* = \xi_j^*(\mathbf{x})$ $(j = 1, 2, ..., l)$ represents the maximum allowable uncertainty magnitudes imposed by the jth behavior function and it is obtained for a fixed set of design variables. During the optimization process, the value of ξ_j^* might be negative, indicating violation of the restriction on the corresponding structural behavior at the nominal value of uncertainties. Therefore, it is necessary to add the signum function when determining the mentioned robust index ξ_j^* $(j = 1, 2, ..., l)$ for each individual behavior function. An example is given here to illustrate this point.

As shown in Fig. 2, a two-bar planar truss subjected to two concentrated forces P_1 and P_2 is considered. The bars have a length of 10 and sectional areas of x_1 and x_2. The Young's module is $E = 1000$. The concentrated forces P_1 and P_2 are uncertain parameters with nominal values $\overline{P}_1 = \overline{P}_2 = 1$. According to (1) one has $z_1 = \left(P_1 - \overline{P}_1\right)/\overline{P}_1 = P_1 - 1$ and $z_2 = \left(P_2 - \overline{P}_2\right)/\overline{P}_2 = P_2 - 1$. The reference variations of the uncertain forces are modeled by an ellipsoid model expressed by $\mathbf{Z} = \left\{\mathbf{z} | \mathbf{z}^{\mathrm{T}} \mathbf{W} \mathbf{z} \le 1\right\}$, where the characteristic matrix

$$\mathbf{W} = \begin{bmatrix} 100 & 0 \\ 0 & 100 \end{bmatrix}.$$

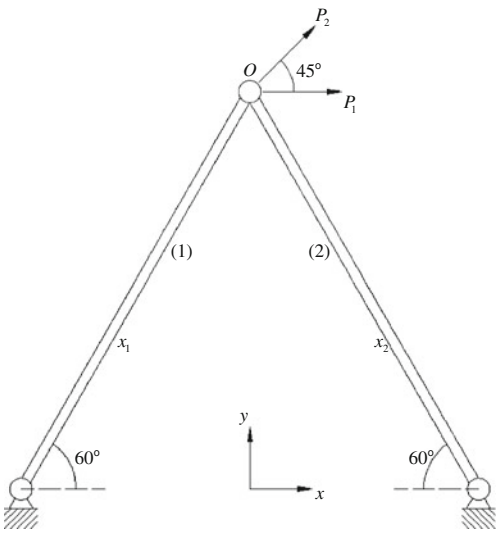

Fig. 2 A two-bar truss subject to two concentrated forces

According to the relation in (4b), the transformation matrix is expressed as

$$\mathbf{T} = \begin{bmatrix} 0.1 & 0 \\ 0 & 0.1 \end{bmatrix}.$$

The horizontal displacement at node O is constrained by $\Delta^{\mathrm{U}} = 0.2$. Thus, the feasibility function for the displacement constraint is expressed as a linear function of the uncertain variables:

$$\begin{aligned} G(\mathbf{x}, \mathbf{z}) = 0.2 &- \frac{1}{100}\left(\frac{1}{x_1} + \frac{1}{x_2}\right)(z_1 + 1) \\ &- \frac{1}{600}\left(\frac{3\sqrt{2} + \sqrt{6}}{x_1} + \frac{3\sqrt{2} - \sqrt{6}}{x_2}\right)(z_2 + 1). \end{aligned}$$

The normalized form of the feasibility function becomes

$$\begin{aligned} g(\mathbf{x}, \boldsymbol{\varphi}) = 0.2 &- \frac{1}{100}\left(\frac{1}{x_1} + \frac{1}{x_2}\right)\left(\frac{\varphi_1}{10} + 1\right) \\ &- \frac{1}{600}\left(\frac{3\sqrt{2} + \sqrt{6}}{x_1} + \frac{3\sqrt{2} - \sqrt{6}}{x_2}\right)\left(\frac{\varphi_2}{10} + 1\right). \end{aligned}$$

Suppose we have two designs $\mathbf{x}_\alpha$ and $\mathbf{x}_\beta$, whose sectional areas are $x_1^\alpha = 0.19$, $x_2^\alpha = 0.19$ and $x_1^\beta = 0.15$, $x_2^\beta = 0.19$, respectively. The ellipsoid model and the feasibility functions for design $\mathbf{x}_\alpha$ and $\mathbf{x}_\beta$ are depicted in the $\boldsymbol{\varphi}$-space, as shown in Fig. 3. In the figure, the circle represents the boundary of the normalized ellipsoid model, and the shaded regions represent the infeasible domains, in which the feasibility function has a negative value. For design $\mathbf{x}_\alpha$, all the combinations of the uncertain loads locate in the feasible domain. However, for design $\mathbf{x}_\beta$, the origin point falls within

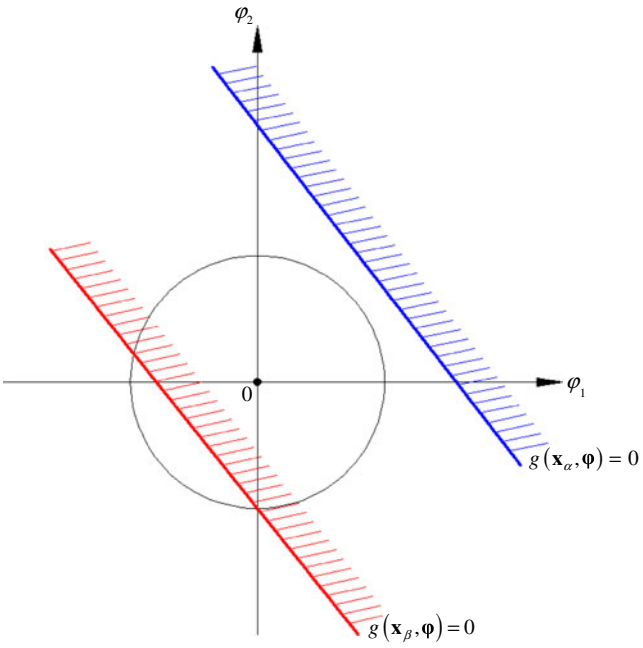

Fig. 3 Ellipsoid model and feasibility functions of design $\mathbf{x}_\alpha$ and $\mathbf{x}_\beta$

the infeasible domain ($g(\mathbf{x}_\beta, \mathbf{0}) < 0$). Therefore, it is necessary to add a negative sign to the distance between the critical curve and the origin point, resulting in a negative robustness index.

3.2 Aggregate function technique

The aforementioned optimization problem is a nested double-level one, with the upper-level problem dealing with the overall structural optimization by maximizing the minimal robustness indices found in the lower level. The non-differentiable nature of this max-min problem brings an extra difficulty. To avoid this difficulty, we employ the aggregate function method, which is also known as the Kreisselmeier–Steinhauser (KS) function method (Kreisselmeier and Steinhauser 1983).

The aggregate function has the following form

$$\widetilde{f}(x) = -\frac{1}{p}\ln\left(\sum_{i=1}^{N} \mathrm{e}^{-pf_i(x)}\right), \tag{13}$$

where $f_i(x)$ $(i = 1, 2, \ldots, N)$ are the concerned functions with N representing the number of these functions, and p is the controlling parameter. One sees that $\lim_{p\to\infty} \widetilde{f}(x) = \min_{i=1\sim N}(f_i(x))$. If p is given a sufficiently large number, the aggregate function $\widetilde{f}(x)$ provides a good smooth approximation of $\min_{i=1\sim N}(f_i(x))$. For demonstrating the aggregate function and the influence of the parameter p, we consider a simple case with two functions, namely $f_1 = -(x-3/2)^2+5/2$ and $f_2 = (x-2)^2+1/2$. As can be seen from Fig. 4, the aggregate function $\widetilde{f}(x)$ forms an envelope of min (f_1, f_2). It is noted that the aggregate function approaches min (f_1, f_2) as p increases, while still maintaining its differentiability. In practice, however, an appropriate value of p should be chosen by making a compromise between the approximation accuracy and the smoothness of the aggregate function.

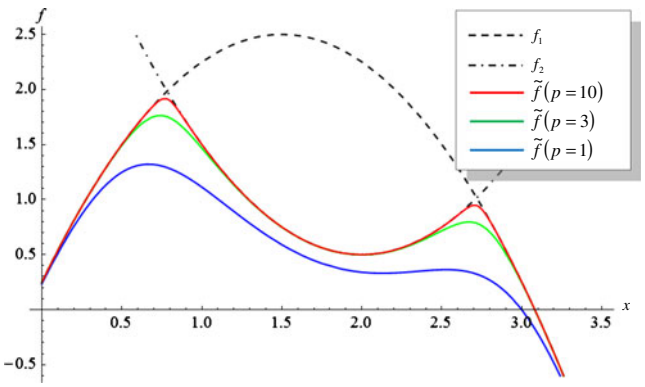

Fig. 4 Envelops of function min (f_1, f_2) with increasing p

With the aggregate function, the objective function in problem (11) is rewritten as

$$\xi^* = -\frac{1}{p}\ln\left(\sum_{k=1}^{l} e^{-p\xi_k^*}\right). \tag{14}$$

4 Numerical implementation

4.1 Sensitivity analysis

In the present study, a gradient-based mathematical programming algorithm is employed for solving the optimization problem, hence the design sensitivity information of the objective function is required. In this section, the computational scheme for sensitivities of the robustness indices with respect to the design variables is derived with the optimum sensitivity analysis technique (Barthelemy and Sobieszczanskisobieski 1983).

Since the lower-level problem (12) has a single constraint, we assume that this constraint is active at the optimum $\boldsymbol{\varphi}^*$, i.e. $g_j(\mathbf{x}, \boldsymbol{\varphi})\big|_{\boldsymbol{\varphi}=\boldsymbol{\varphi}^*} = 0$. From the Karush–Kuhn–Tucker optimality condition, it holds that

$$\left(\frac{\partial \xi_j^*}{\partial \boldsymbol{\varphi}} + \lambda\frac{\partial g_j}{\partial \boldsymbol{\varphi}}\right)\Bigg|_{\boldsymbol{\varphi}=\boldsymbol{\varphi}^*} = \mathbf{0}, \tag{15}$$

where λ is the Lagrangian multiplier.

We assume that the behavior constraint of the lower-level problem remains active at the optimum $\boldsymbol{\varphi}^*$ under any perturbation of the design variable $\mathbf{x}$, which leads to

$$\frac{\mathrm{d}g_j}{\mathrm{d}\mathbf{x}}\Bigg|_{\boldsymbol{\varphi}=\boldsymbol{\varphi}^*} = \left(\frac{\partial g_j}{\partial \mathbf{x}} + \left(\frac{\partial \boldsymbol{\varphi}}{\partial \mathbf{x}}\right)^{\mathrm{T}}\frac{\partial g_j}{\partial \boldsymbol{\varphi}}\right)\Bigg|_{\boldsymbol{\varphi}=\boldsymbol{\varphi}^*} = \mathbf{0}. \tag{16}$$

Left-multiplying (15) with matrix $(\partial\boldsymbol{\varphi}/\partial\mathbf{x})^{\mathrm{T}}$, it yields

$$\left(\left(\frac{\partial \boldsymbol{\varphi}}{\partial \mathbf{x}}\right)^{\mathrm{T}}\frac{\partial \xi_j^*}{\partial \boldsymbol{\varphi}} + \lambda\left(\frac{\partial \boldsymbol{\varphi}}{\partial \mathbf{x}}\right)^{\mathrm{T}}\frac{\partial g_j}{\partial \boldsymbol{\varphi}}\right)\Bigg|_{\boldsymbol{\varphi}=\boldsymbol{\varphi}^*} = \mathbf{0} \tag{17}$$

Combining (16) and (17), one has

$$\left(\left(\frac{\partial \boldsymbol{\varphi}}{\partial \mathbf{x}}\right)^{T}\frac{\partial \xi_j^*}{\partial \boldsymbol{\varphi}}\right)\Bigg|_{\boldsymbol{\varphi}=\boldsymbol{\varphi}^*} = \lambda\,\frac{\partial g_j}{\partial \mathbf{x}}\Bigg|_{\boldsymbol{\varphi}=\boldsymbol{\varphi}^*}. \tag{18}$$

Thus, the derivative of ξ_j^* with respect to the design variables becomes

$$\frac{\mathrm{d}\xi_j^*}{\mathrm{d}\mathbf{x}} = \left(\left(\frac{\partial \boldsymbol{\varphi}}{\partial \mathbf{x}}\right)^{\mathrm{T}}\frac{\partial \xi_j^*}{\partial \boldsymbol{\varphi}}\right)\Bigg|_{\boldsymbol{\varphi}=\boldsymbol{\varphi}^*} = \lambda\,\frac{\partial g_j}{\partial \mathbf{x}}\Bigg|_{\boldsymbol{\varphi}=\boldsymbol{\varphi}^*}. \tag{19}$$

In (19), the Lagrangian multiplier λ is available as a by-product of the lower-level optimization and the derivative of the behavior function $\partial g_j/\partial\mathbf{x}$ can be easily computed by using the adjoint sensitivity method as usual. Therefore $\mathrm{d}\xi_j^*/\mathrm{d}\mathbf{x}$ can be obtained without much additional computational effort.

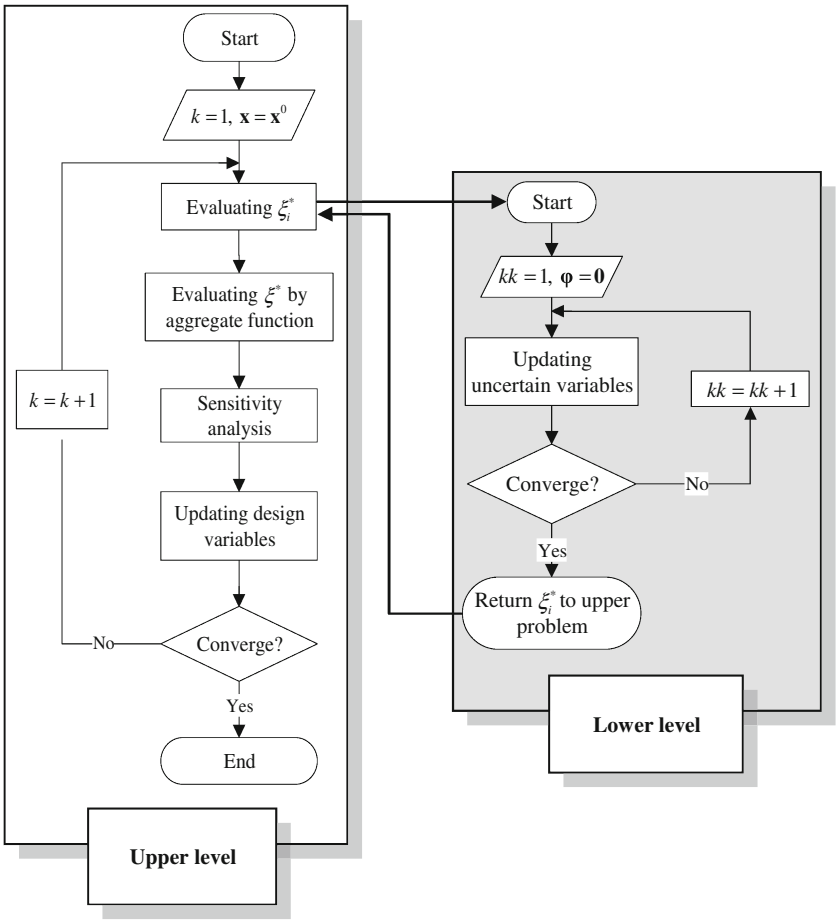

Fig. 5 Flowchart for solving the nested optimization problem

4.2 Optimization algorithms and flowchart

In this study, the upper-level optimization problem is solved by the conservative convex separable approximation-based GCMMA (Global Convergence Method of Moving Asymptotes) algorithm developed by Svanberg (2001, 2007), and the lower-level problem is solved by the *fmincon* function of the Matlab® Optimization Toolbox™. The flowchart for solving the nested optimization problem is depicted in Fig. 5. In the figure, the left side is the upper level problem, which solves the structural optimization problem; and the right side is the lower level problem, which evaluates the robustness indices of the structural performance functions.

5 Numerical examples

For illustrating the validity of the proposed robust design optimization formulation and the numerical techniques, three examples are given in this section. The first one regards the optimal truss design problem under bar cross-sectional areas fluctuation, the second one copes with the problem with material property uncertainty, and the third one concerns the problem under loading uncertainty. The parameter p in the aggregated objective function is set as 10 in all the examples. The change of objective function value with respect to the previous iteration step is chose as the convergence criteria. and the optimization is terminated if this change is less than 0.001.

5.1 Optimal design of a five-bar planar truss

Geometrical parameter uncertainties are common in practical engineering due to the manufacturing error. In the first example, the size optimization of a five-bar planar truss structure subjected to concentrated forces with uncertain cross-sectional areas is considered (see Fig. 6). The Young's modulus is $E = 200$. The truss is subject to a horizontal force $P_1 = 10$ and a vertical force $P_2 = 10$ at node 3. The cross-sectional areas are uncertain-but-bounded parameters and modeled by an ellipsoid model expressed as $\mathbf{Z} = \left\{\mathbf{z}|\mathbf{z}^{\mathrm{T}}\mathbf{W}\mathbf{z} \le 1\right\}$, where $\mathbf{W} = 100 \times \mathrm{diag}(1, 1, 1, 1, 1)$. According to the transformation defined in (4b), a point-to-set function is defined as $\mathbf{z} \in \left\{\mathbf{z} \in \Re^5 | \mathbf{z} = \xi\mathbf{T}\boldsymbol{\varphi}, \|\boldsymbol{\varphi}\|_2 \le 1, \boldsymbol{\varphi} \in \Re^5\right\}$, with the transformation matrix being $\mathbf{T} = 0.1 \times \mathbf{I}$. Here $\mathbf{I} \in \Re^{5\times5}$ is an

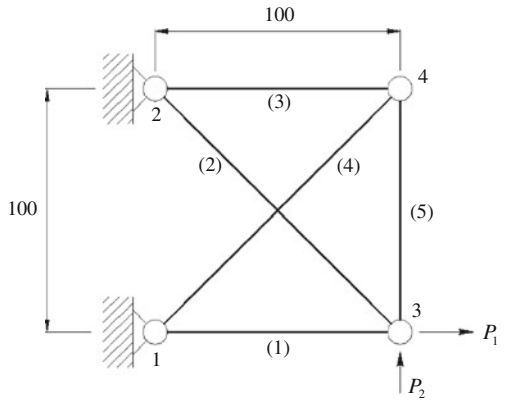

Fig. 6 A five-bar planar truss subjected to concentrated forces

identity matrix. The horizontal and vertical displacements of node 3 are restricted by $u_3 \leq 1.6$ and $v_3 \leq 2.8$, respectively. Let $\xi^*_{u_3}$ and $\xi^*_{v_3}$ denote the robustness indices of the horizontal and vertical displacements at node 3, respectively. The design objective is to maximize the smaller one of these two robustness indices. In this example, the nominal values of the cross-sectional areas are treated as design variables and they have initial values $x_i^0 = 5.0$ $(i = 1, 2, \ldots, 5)$ and lower/upper bound limits $x_i^{\mathrm{L}} = 0.01$, $x_i^{\mathrm{U}} = 40.00$ $(i = 1, 2, \ldots, 5)$. Three cases of displacement requirement and volume constraint considered in this example are listed in Table 1.

The optimal results obtained from robust design optimization are listed in Table 2, where the bolded numbers indicate the smaller one of the robustness indices $\xi^*_{u_3}$ and $\xi^*_{v_3}$ achieved in the final design. The optimized structure is shown in Fig. 7, in which the line thickness schematically represents the cross-sectional areas of the member bars. From the optimization results one sees that better robustness can be achieved with larger material volume. For comparison, nominal value-based deterministic optimization is also carried out, where the material volume is minimized under the same displacement constraints $u_3 \leq 1.6$ and $v_3 \leq 2.8$. For the deterministic optimal solution given in Table 2, the robustness index for the displacement v_3 is zero. This

Table 1 Displacement requirements and material volume constraints for the five-bar truss

	u_3	v_3	Volume
Case 1	1.6	2.8	2260
Case 2	1.6	2.8	2450
Case 3	1.6	2.8	2680

Table 2 Optimal solutions for the five-bar truss

Member number	Cross-sectional area				
	Initial design	Optimal design			
		Deterministic	Case 1	Case 2	Case 3
1	5.0	8.61	9.26	9.90	10.57
2	5.0	8.61	9.40	10.27	11.34
3	5.0	0.01	0.01	0.02	0.05
4	5.0	0.02	0.02	0.03	0.07
5	5.0	0.01	0.01	0.02	0.05
$\xi^*_{u_3}$	1.10	2.75	3.25	3.69	4.11
$\xi^*_{v_3}$	**0.78**	**0.00**	**1.09**	**2.07**	**3.06**
Volume	2914	2084	2260	2450	2680

indicates that the structure is safe only when the uncertain parameters take nominal values, and any perturbation to these parameters will cause violation of the displacement constraints.

In order to verify the predicted robustness of the optimal designs obtained with the present method, Monte Carlo simulations, each with 200000 samples taken from the ellipsoid model, were carried out on the optimized structures for the three cases. Therein, the variations of the uncertain parameter were scaled by a factor of $\min\left(\xi^*_{u_3}, \xi^*_{v_3}\right)$. The simulation results are shown in Fig. 8.

In Fig. 8a∼f, the tail distributions of the concerned displacements are amplified in order to provide a clearer view. It can be seen that no violation of the displacement requirements occurs when the uncertain variation is scaled by the smaller robustness index, and this thus verifies the predicted robustness indices of the obtained optimal designs.

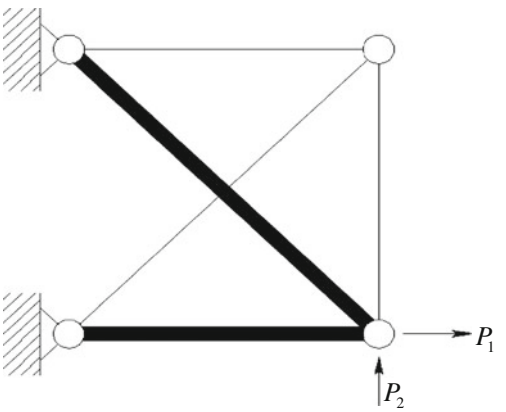

Fig. 7 Optimized five-bar truss structure

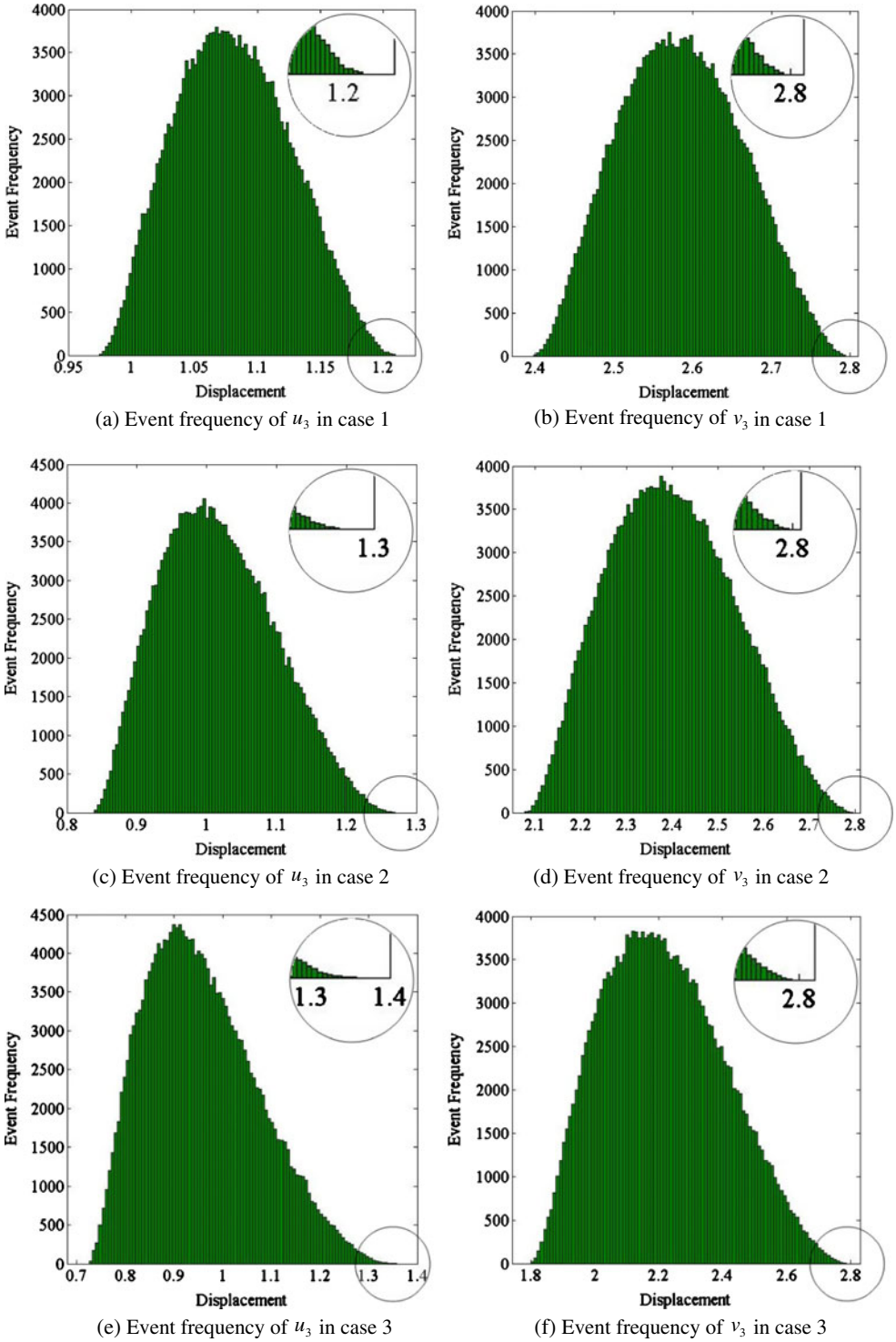

Fig. 8 Monte Carlo simulation results

(a) Event frequency of u_3 in case 1

(b) Event frequency of v_3 in case 1

(c) Event frequency of u_3 in case 2

(d) Event frequency of v_3 in case 2

(e) Event frequency of u_3 in case 3

(f) Event frequency of v_3 in case 3

5.2 Optimal design of a ten-bar planar truss

The robust optimization of a ten-bar truss structure exhibiting material property uncertainty is considered in this example. The structure and the loading condition are shown in Fig. 9. Two concentrated forces $P_1 = 100$ and $P_2 = 100$ are applied at node 6 and node 4, respectively. We divide the bars into two groups (see Table 3) and suppose that all the bars within each group have the same Young's modulus. The Young's moduli of both groups of bars E_1 and E_2

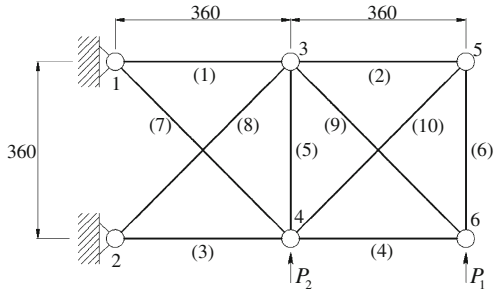

Fig. 9 A ten-bar planar truss subjected to concentrated forces

Table 3 Bar grouping and nominal values of Young's moduli for each group

	Bar group 1	Bar group 2
Bar no.	(1)∼(6)	(7)∼(10)
Nominal value	$\overline{E}_1 = 10000$	$\overline{E}_2 = 8000$

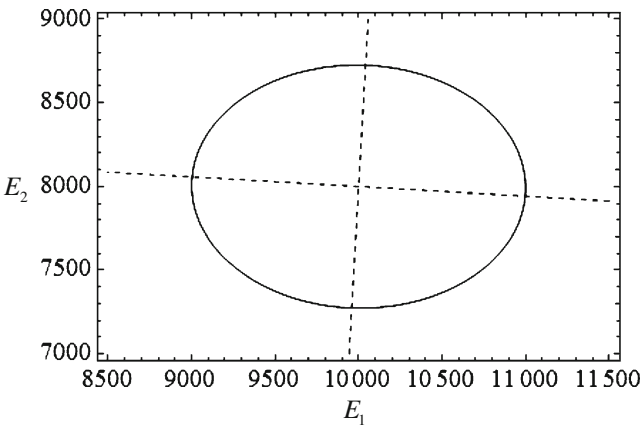

Fig. 10 The convex model for grouped Young's moduli uncertainties

Table 4 Displacement requirements and material volume constraints for the ten-bar truss

	v_3	v_6	Volume
Case 1	2.0	5.0	22700
Case 2	2.0	5.0	24500
Case 3	2.0	5.0	26500

Table 5 Optimal solutions for the ten-bar truss

Member number	Cross-sectional area				
	Initial design	Optimal design			
		Deterministic	Case 1	Case 2	Case 3
1	7	13.06	14.03	15.21	16.57
2	7	0.01	0.01	0.01	0.01
3	7	9.04	9.71	10.54	11.49
4	7	6.48	6.96	7.55	8.22
5	7	0.01	0.01	0.01	0.01
6	7	0.01	0.01	0.01	0.01
7	7	0.71	0.73	0.76	0.78
8	7	10.44	11.16	12.00	12.90
9	7	10.24	10.95	11.79	12.68
10	7	0.01	0.01	0.01	0.01
$\xi^*_{v_3}$	**−5.53**	1.06	1.90	2.74	3.49
$\xi^*_{v_6}$	−3.46	**0.00**	**1.00**	**2.04**	**3.02**
Volume	29375	21195	22700	24500	26500

are unknown-but-bounded parameters, with their nominal values listed in Table 3. The uncertain Young's moduli are modeled by an ellipsoid model, in which the characteristic matrix is

$$\mathbf{W} = \begin{bmatrix} 100 & 1.21 \\ 1.21 & 121 \end{bmatrix}.$$

The transformation matrix is thus expressed by using the relation in (4b) as

$$\mathbf{T} = \begin{bmatrix} -0.09987 & 0.00521 \\ 0.00574 & 0.09073 \end{bmatrix}.$$

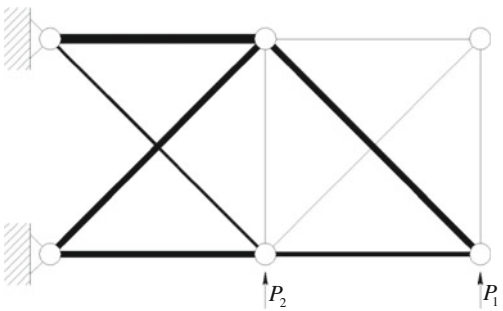

Fig. 11 Optimized ten-bar truss structure

Since the ellipsoid model is written as

$$\left\{\begin{pmatrix} E_1 \\ E_2 \end{pmatrix} \middle| \begin{pmatrix} \frac{E_1-10000}{10000} & \frac{E_2-8000}{8000} \end{pmatrix} \begin{bmatrix} 100 & 1.21 \\ 1.21 & 121 \end{bmatrix} \times \begin{pmatrix} \frac{E_1-10000}{10000} & \frac{E_2-8000}{8000} \end{pmatrix}^{\mathrm{T}} \le 1 \right\},$$

the corresponding standard equation describing the ellipse boundary is

$$1.563\times10^{-8}E_1^2 + 1.891\times10^{-8}E_2^2 + 3.781\times10^{-10}E_1E_2 - 3.163\times10^{-4}E_1 - 3.819\times10^{-4}E_2 + 3.491 = 0.$$

This ellipse is depicted in Fig. 10 to demonstrate the convex model of the uncertainties.

The vertical displacements at node 3 and node 6 are restricted by $v_3 \le 2.0$ and $v_6 \le 5.0$ respectively, and the corresponding robustness indices are denoted by $\xi^*_{v_3}$ and $\xi^*_{v_6}$. The cross-sectional areas of the member bars are considered as design variables, with lower limits $x_i^{\mathrm{L}} = 0.01$, upper limits $x_i^{\mathrm{U}} = 40.00$ and initial values $x_i^0 = 20.00$ $(i = 1, 2, \ldots, 10)$.

Three cases of displacement requirement and material volume constraint considered are listed in Table 4. The results of robust design optimization and deterministic optimization are listed in Table 5, in which the numbers in bold font represent the smaller robustness indices. The optimal design is shown in Fig. 11. Obviously, if the member bars reaching lower bound limit values of cross-sectional area are removed, one gets a statically determinant truss. It should be noted that the robustness index $\xi^*_{v_3}$ and $\xi^*_{v_6}$ are both negative for the initial design, which means the initial design is infeasible when the Young's moduli E_1 and E_2 take their nominal values. In the deterministic optimal result achieved by minimizing the material volume under the corresponding displacement constraints, the zero-valued robustness index for $\mathbf{v}_6$ implies that the displacement requirements cannot be satisfied when E_1 and E_2 have variations around their nominal values.

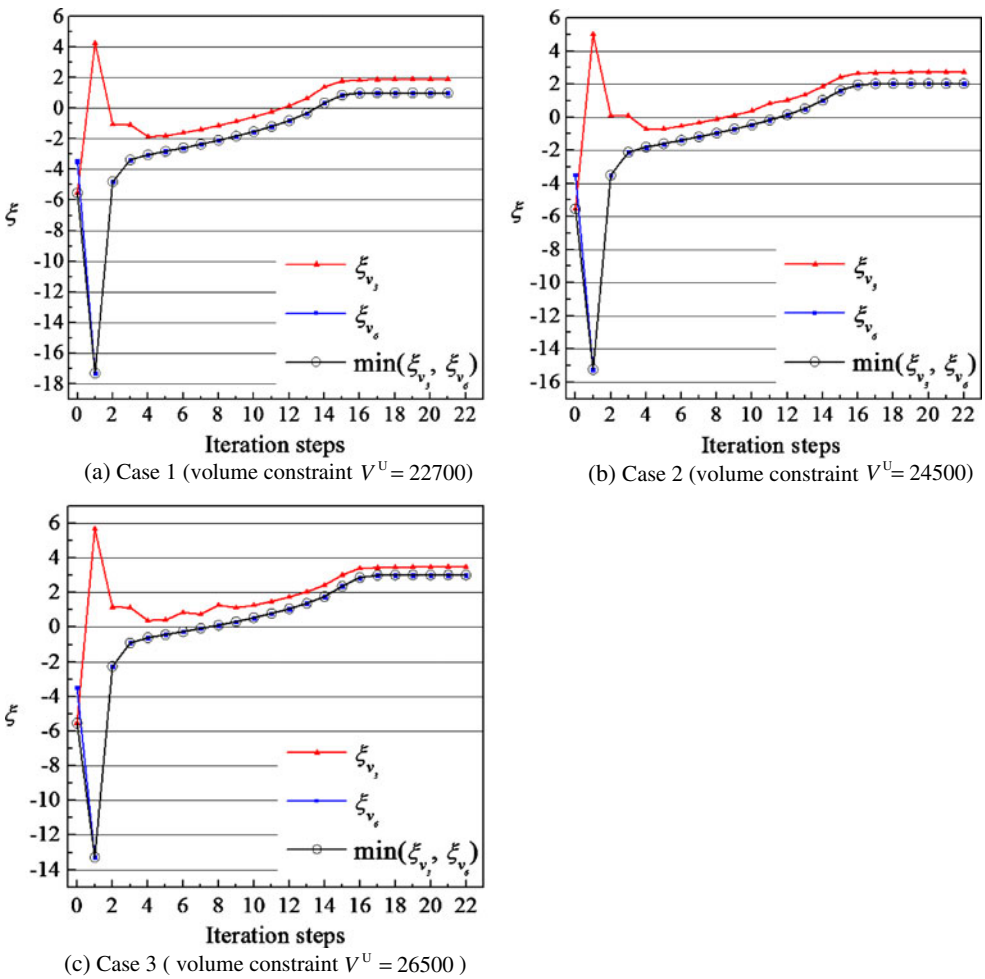

(a) Case 1 (volume constraint $V^{\mathrm{U}} = 22700$)

(b) Case 2 (volume constraint $V^{\mathrm{U}} = 24500$)

(c) Case 3 (volume constraint $V^{\mathrm{U}} = 26500$)

Fig. 12 Iteration histories of ten-bar truss optimization

The iteration histories of the optimization process in this example are plotted in Fig. 12, which show a stable convergence as well as a steady increase of the objective function after a few first iteration steps required for searching for a feasible solution.

Monte Carlo simulations with 200000 samples were carried out on the three cases to verify the robustness of the optimal designs. In each simulation, the variation of grouped uncertain Young's moduli was scaled by $\min\left(\xi_{v_3}^*, \xi_{v_6}^*\right)$. Simulation results are given in Fig. 13, from

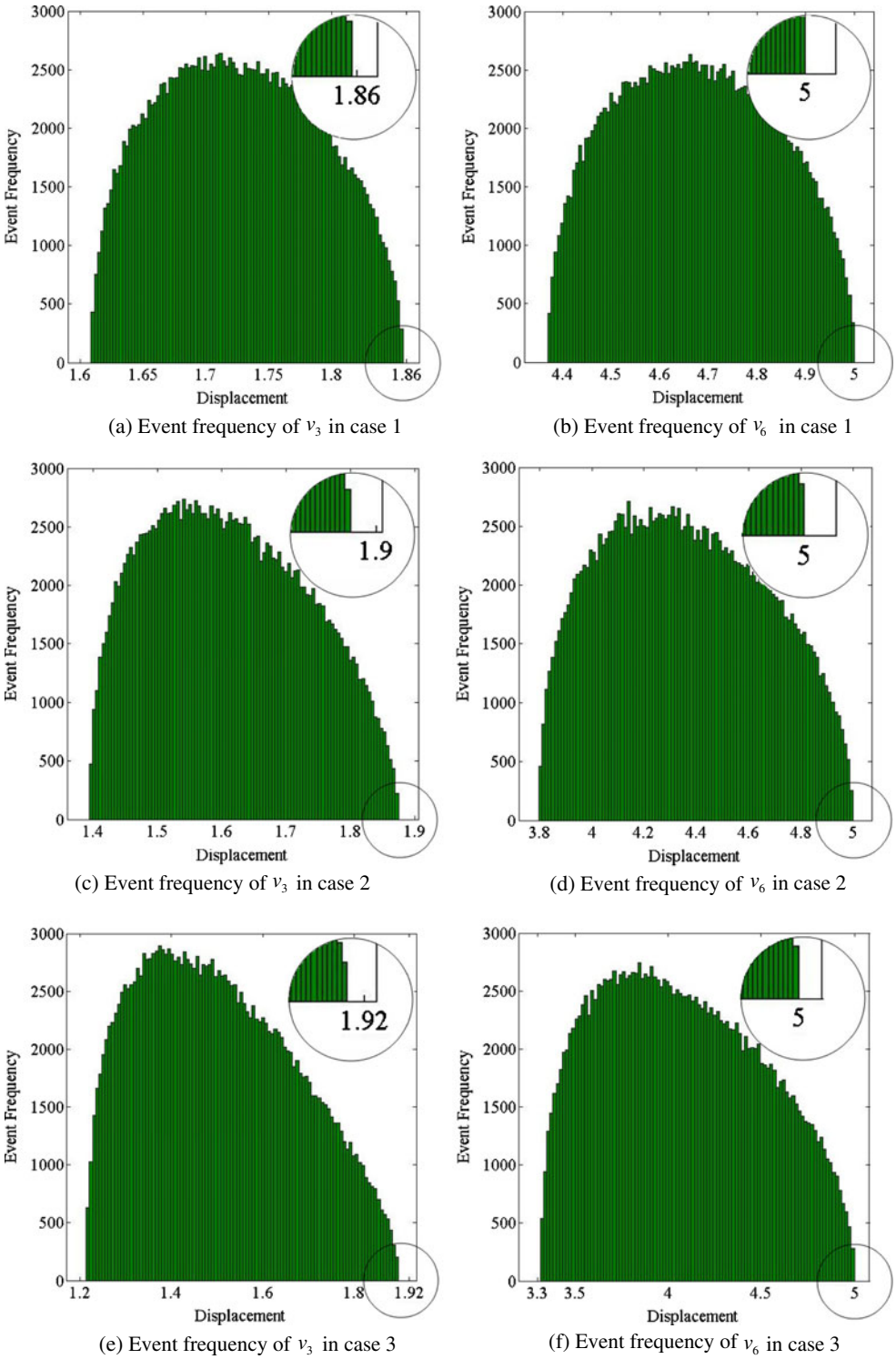

Fig. 13 Monte Carlo simulation results

(a) Event frequency of v_3 in case 1

(b) Event frequency of v_6 in case 1

(c) Event frequency of v_3 in case 2

(d) Event frequency of v_6 in case 2

(e) Event frequency of v_3 in case 3

(f) Event frequency of v_6 in case 3

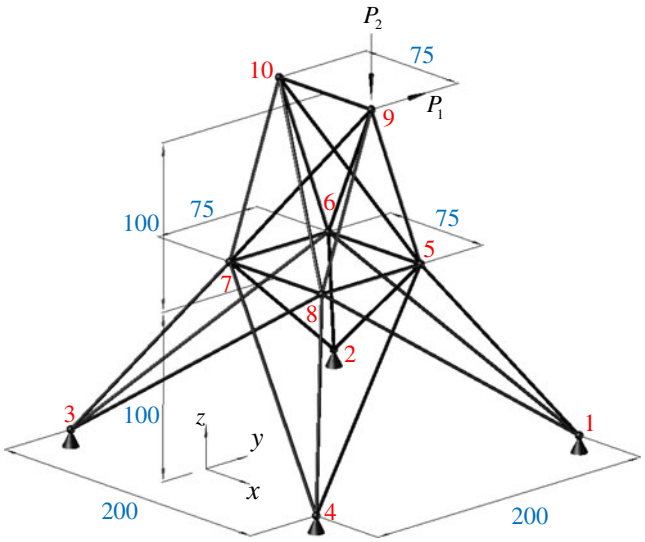

Fig. 14 A twenty-five-bar space truss subjected to concentrated forces

which no displacement violation is observed. Hence, the feasibility of the obtained optimal structures under specified uncertainty can be ensured.

5.3 Optimal design of a 25-bar space truss

In this example, the robust optimization of a 25-bar space truss against material property and load uncertainty is considered. The geometrical dimensions of the structure and the loads are given in Fig. 14. The element-node connectivity for the truss is listed in Table 6. The 25 bars are divided into two groups, and all the bars within each group have the same Young's modulus which is represented by E_1 and E_2 respectively. The Young's moduli E_1 and E_2 are unknown-but-bounded parameters and their nominal values are listed in Table 7. Two concentrated forces P_1 and P_2 which are also unknown-but-bounded parameters are applied to node 9 along y-directional and z-directional, respectively. The nominal values of the force magnitudes are $\overline{P}_1 = 100$ and $\overline{P}_2 = -50$.

Table 7 Bar grouping and nominal values of Young's moduli for each group

	Bar group 1	Bar group 2
Bar no.	(1)∼(13)	(14)∼(25)
Nominal value	$\overline{E}_1 = 1500$	$\overline{E}_2 = 2000$

We use a single ellipsoid model to describe the reference variations of the Young's moduli and the loads, with the characteristic matrix being

$$\mathbf{W} = \begin{bmatrix} 350 & 20 & 0 & 0 \\ 20 & 200 & 20 & 0 \\ 0 & 20 & 180 & 20 \\ 0 & 0 & 20 & 250 \end{bmatrix}.$$

The corresponding transformation matrix is

$$\mathbf{T} = \begin{bmatrix} 0.04150 & -0.00834 & -0.00122 & -0.05278 \\ -0.03865 & 0.05924 & 0.00576 & -0.00702 \\ 0.06607 & 0.03169 & 0.01730 & -0.00083 \\ -0.01530 & -0.01505 & 0.05980 & -0.00016 \end{bmatrix}.$$

The y-directional and the z-directional displacements at the loading point are restricted by $v_9 \leq 3.5$ and $w_9 \geq -0.28$, as shown in Table 8. Three cases of displacement requirement and volume constraint are also listed in Table 8. The bar cross-sectional areas x_i $(i = 1, 2, \ldots, 25)$ are treated as design variables, with bound limits $0.01 \leq x_i \leq 40.00$ $(i = 1, 2, ..., 25)$ and initial values $x_i^0 = 10.00$ $(i = 1, 2, ..., 25)$. The optimal results of the robust design optimization, as well as the deterministic optimization for minimizing the material volume under displacement constraints, are given in Table 9. Therein, the bolded numbers indicate the smaller one of the two robustness indices. Again, in the deterministic optimization results, $\xi_{v_9}^* = 0$ implies the optimal structure can only assure structural

Table 6 Element-node connectivity for twenty-five-bar truss

Bar	1	2	3	4	5	6	7	8	9	10	11	12	13
Node	9,10	7,10	8,9	5,9	6,10	8,10	7,9	6,9	5,10	5,6	6,7	7,8	5,8

Bar	14	15	16	17	18	19	20	21	22	23	24	25
Node	3,7	4,8	1,5	2,6	4,7	3,8	1,8	4,5	2,5	1,6	3,6	2,7

Table 8 Displacement requirements and material volume constraints for the twenty-five-bar truss

	v_9	w_3	Volume
Case 1	3.5	−0.28	15000
Case 2	3.5	−0.28	18000
Case 3	3.5	−0.28	20000

safety when the uncertain parameters take nominal values. It should be noted that, the robustness index of ξ^*_{w9} in the initial design is negative, which means the initial design is infeasible even for the nominal Young's moduli and loading condition. The optimal structure is shown in Fig. 15, with dashed lines representing the bars with sectional areas reaching the lower bounds.

The computational efficiency of the present method is also studied in this example. The number of iterations involved in solving the upper level and the lower level problem, together with computing time, are listed in Table 10. In these constraint cases, it takes an average of 7.1, 7.2 and 7.6 iterations (maximum 8) respectively for the lower level problem to converge to a solution by the *fmincon* optimizer. For the upper level problem, it takes the GCMMA optimizer 64 iterations for constraint case 1 and 3, and 62 iterations for case 2 to converge to the optimal solution. The total computing time is also reasonable in all three cases.

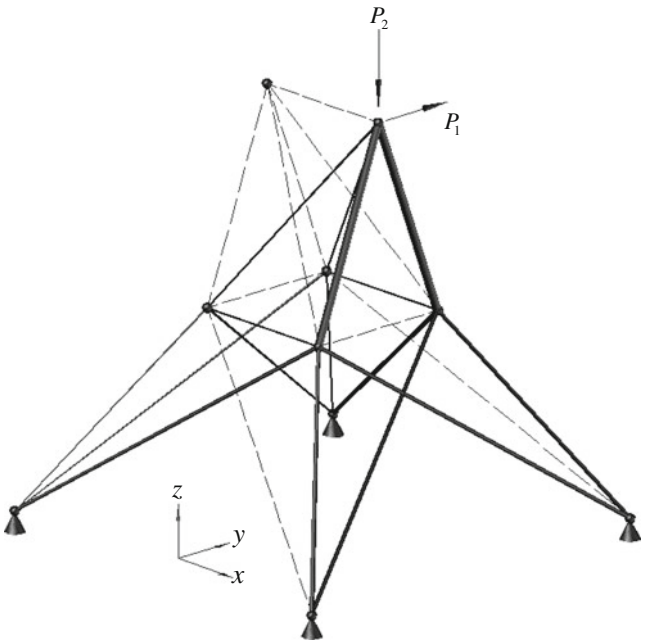

Fig. 15 Optimized twenty-five-bar truss structure

Table 9 Optimal results for the twenty-five-bar truss

Member number	Cross-sectional area				
	Initial design	Optimal design			
		Deterministic	Case 1	Case 2	Case 3
1	10	0.01	0.01	0.01	0.01
2	10	0.01	0.01	0.01	0.01
3	10	17.24	23.11	26.07	28.40
4	10	20.88	27.58	30.65	33.08
5	10	0.01	0.01	0.01	0.01
6	10	0.01	0.01	0.01	0.01
7	10	0.24	0.11	0.17	0.23
8	10	0.24	0.11	0.17	0.23
9	10	0.01	0.01	0.01	0.01
10	10	0.02	0.01	0.01	0.02
11	10	0.01	0.01	0.01	0.01
12	10	0.02	0.01	0.01	0.02
13	10	0.01	0.01	0.01	0.01
14	10	0.22	0.09	0.15	0.20
15	10	12.10	14.33	16.73	18.88
16	10	14.66	17.11	19.69	22.02
17	10	0.22	0.09	0.15	0.20
18	10	0.01	0.01	0.01	0.01
19	10	9.15	10.82	12.64	14.26
20	10	3.65	4.33	5.05	5.70
21	10	4.42	5.16	5.94	6.65
22	10	11.08	12.91	14.86	16.63
23	10	0.01	0.01	0.01	0.01
24	10	0.04	0.02	0.03	0.04
25	10	0.04	0.02	0.03	0.04
ξ^*_{v9}	2.10	**0.00**	**1.07**	**2.55**	**3.73**
ξ^*_{w9}	**−0.62**	2.86	7.26	8.17	8.86
Volume	33072	12919	15700	18000	20000

Table 10 Number of iterations and computing time

	Number of iterations		Computing time (second)
	Lower level problem (average)	Upper level problem	
Case 1	7.1	64	16
Case 2	7.2	62	21
Case 3	7.6	64	23

6 Conclusions and discussions

In practical circumstances where precise probabilistic distribution of uncertain parameters is unavailable but their bounds can be identified, convex models provide an alternative description of these uncertainties. This paper investigates robust optimization of truss structures with unknown-but-bounded parameters and loading conditions using ellipsoid convex models. Therein, a quantified measure of robustness is proposed, and the design objective is to maximize the minimum one of the robustness indices for the concerned structural performance requirements. The aggregate function technique is employed for circumventing the difficulty in treating the max-min type objective function of the upper-level problem. The sensitivity analysis scheme is derived based on the optimum sensitivity analysis technique. Three numerical examples of truss structures were treated with the present formulation, and the results showed the validity of the proposed method. The robustness of the obtained optimal designs was also verified by Monte Carlo simulations.

In this study, the lower-level problem is solved with a mathematical programming algorithm. However, the HL-RF iteration scheme widely used in probabilistic reliability analysis can also be adapted and employed for obtaining the robustness index in the lower-level problem. Moreover, it is still worthwhile to further investigate more efficient numerical techniques for solving the nested double level optimization problem.

Though only displacements of truss structures are treated in the numerical examples, the proposed problem statement and numerical techniques can be easily extended to robust design optimization for more general behaviors of other types of structures with uncertainties.

Acknowledgements The support from the Major Project of Chinese National Programs for Fundamental Research and Development (Grant 2010CB832703) and the Natural Science Foundation of China (Grant 91130025, 11072047) is gratefully acknowledged.

References

Asadpoure A, Tootkaboni M, Guest JK (2011) Robust topology optimization of structures with uncertainties in stiffness—application to truss structures. Comput Struct 89(11–12):1131–1141. doi:10.1016/j.compstruc.2010.11.004

Barthelemy JFM, Sobieszczanskisobieski J (1983) Optimum sensitivity derivatives of objective functions in non-linear programming. AIAA J 21(7):913–915

Beck AT, de Santana Gomes WJ (2010) On structural design optimization under uncertainty and risk. IOP Conf Ser: Mater Sci Eng 10:012110–012193

Ben-Haim Y, Elishakoff I (1990) Convex models of uncertainty in applied mechanics. Elsevier, Amsterdam

Ben-Tal A, Nemirovski A (1997) Robust truss topology design via semidefinite programming. SIAM J Optim 7(4):991–1016

Beyer HG, Sendhoff B (2007) Robust optimization—a comprehensive survey. Comput Methods Appl Mech Eng 196(33–34):3190–3218

Chen SK, Chen W (2011) A new level-set based approach to shape and topology optimization under geometric uncertainty. Struct Multidisc Optim 44(1):1–1818

Chen SK, Chen W, Lee SH (2010) Level set based robust shape and topology optimization under random field uncertainties. Struct Multidisc Optim 41(4):507–524

Chen W, Lewis K (1999) Robust design approach for achieving flexibility in multidisciplinary design. AIAA J 37(9):982–989

Chen W, Allen JK, Mavris DN, Mistree F (1996a) A concept exploration method for determining robust top-level specifications. Eng Optim 26(2):137–158

Chen W, Allen JK, Tsui KL, Mistree F (1996b) A procedure for robust design: minimizing variations caused by noise factors and control factors. J Mech Des 118(4):478–485

Chen W, Sahai A, Messac A, Sundararaj GJ (2000) Exploration of the effectiveness of physical programming in robust design. J Mech Des 122(2):155–163

Doltsinis I, Kang Z (2004) Robust design of structures using optimization methods. Comput Methods Appl Mech Eng 193 (23–26):2221–2237

Doltsinis I, Kang Z (2006) Perturbation-based stochastic FE analysis and robust design of inelastic deformation processes. Comput Methods Appl Mech Eng 195(19–22):2231–2251

Du L, Choi KK, Youn BD (2006) Inverse possibility analysis method for possibility-based design optimization. AIAA J 44(12):2682–2690

Elishakoff I (1995) Essay on uncertainties in elastic and viscoelastic structures: from A. M. Freudenthal's criticisms to modern convex modeling. Comput Struct 56(7):871–895

Elishakoff I (1999) Are probabilistic and anti-optimization approaches compatible? In: Elishakoff I (ed) Whys and hows in uncertainty modelling: probability, fuzziness and anti-optimization. Springer, New York, pp 263–341

Elseifi MA, Gurdal Z, Nikolaidis E (1999) Convex/probabilistic models of uncertainties in geometric imperfections of stiffened composite panels. AIAA J 37(4):468–474

Erfani T, Utyuzhnikov SV (2012) Control of robust design in multi-objective optimization under uncertainties. Struct Multidisc Optim 45(2):247–256

Ganzerli S, Pantelides CP (2000) Optimum structural design via convex model superposition. Comput Struct 74(6):639–647

Guest JK, Igusa T (2008) Structural optimization under uncertain loads and nodal locations. Comput Methods Appl Mech Eng 198(1):116–124

Han X, Jiang C, Gong S, Huang YH (2008) Transient waves in composite-laminated plates with uncertain load and material property. Int J Numer Methods Eng 75(3):253–274

Harzheim L, Warnecke U (2010) Robustness optimization of the position of an anti-roll bar link to avoid the toggling of a rear axle stabilizer. Struct Multidisc Optim 42(2):315–323

Hu JX, Qiu ZP (2010) Non-probabilistic convex models and interval analysis method for dynamic response of a beam with bounded uncertainty. Appl Math Model 34(3):725–734

Impollonia N, Muscolino G (2011) Interval analysis of structures with uncertain-but-bounded axial stiffness. Comput Methods Appl Mech Eng 200(21–22):1945–1962

Jiang C, Han X, Liu GR (2007) Optimization of structures with uncertain constraints based on convex model and satisfaction degree of interval. Comput Methods Appl Mech Eng 196(49–52):4791–4800

Jiang C, Han X, Liu GR, Liu GP (2008) A nonlinear interval number programming method for uncertain optimization problems. Eur J Oper Res 188(1):1–13

Jiang C, Han X, Lu GY, Liu J, Zhang Z, Bai YC (2011) Correlation analysis of non-probabilistic convex model and corresponding structural reliability technique. Comput Methods Appl Mech Eng 200(33–36):2528–2546. doi:10.1016/j.cma.2011.04.007

Kang Z, Luo YJ (2009) Non-probabilistic reliability-based topology optimization of geometrically nonlinear structures using convex models. Comput Methods Appl Mech Eng 198(41–44):3228–3238

Kang Z, Luo YJ (2010) Reliability-based structural optimization with probability and convex set hybrid models. Struct Multidisc Optim 42(1):89–102

Kanno Y, Takewaki I (2006) Sequential semidefinite program for maximum robustness design of structures under load uncertainty. J Optim Theory Appl 130(2):265–287

Kreisselmeier G, Steinhauser R (1983) Application of vector performance optimization to a robust-control loop design for a fighter aircraft. Int J Control 37(2):251–284

Lagaros ND, Papadrakakis M (2007) Robust seismic design optimization of steel structures. Struct Multidisc Optim 33(7):457–469

Lagaros ND, Plevris V, Papadrakakis M (2005) Multi-objective design optimization using cascade evolutionary computations. Comput Methods Appl Mech Eng 194(30–33):3496–3515

Lagaros ND, Plevris V, Papadrakakis M (2010) Neurocomputing strategies for solving reliability-robust design optimization problems. Eng Comput 27(8):819–840

Lombardi M, Haftka RT (1998) Anti-optimization technique for structural design under load uncertainties. Comput Methods Appl Mech Eng 157(1–2):19–31

Luo YJ, Kang Z, Luo Z, Li A (2009) Continuum topology optimization with non-probabilistic reliability constraints based on multi-ellipsoid convex model. Struct Multidisc Optim 39(3):297–310

Moller B, Beer M (2008) Engineering computation under uncertainty—capabilities of non-traditional models. Comput Struct 86(10):1024–1041

Mourelatos ZP, Zhou J (2005) Reliability estimation and design with insufficient data based on possibility theory. AIAA J 43(9):1696–1705

Pantelides CP, Ganzerli S (1998) Design of trusses under uncertain loads using convex models. J Struct Eng 124(3):318–329

Papadrakakis M, Lagaros ND, Plevris V (2005) Design optimization of steel structures considering uncertainties. Eng Struct 27(10):1408–1418

Parkinson A (1995) Robust mechanical design using engineering models. J Mech Des 117:48–54

Qiu ZP (2003) Comparison of static response of structures using convex models and interval analysis method. Int J Numer Methods Eng 56(12):1735–1753

Qiu ZP (2005) Convex models and interval analysis method to predict the effect of uncertain-but-bounded parameters on the buckling of composite structures. Comput Methods Appl Mech Eng 194(18–20):2175–2189

Sandgren E, Cameron TM (2002) Robust design optimization of structures through consideration of variation. Comput Struct 80(20–21):1605–1613

Schueller GI, Jensen HA (2008) Computational methods in optimization considering uncertainties—an overview. Comput Methods Appl Mech Eng 198(1):2–13

Sigmund O (2009) Manufacturing tolerant topology optimization. Acta Mech Sinica 25(2):227–239

Sun G, Li G, Zhou S, Li H, Hou S, Li Q (2011) Crashworthiness design of vehicle by using multiobjective robust optimization. Struct Multidisc Optim 44(1):99–110

Svanberg K (2001) A class of globally convergent optimization methods based on conservative convex separable approximations. SIAM J Optim 12(2):555–573

Svanberg K (2007) MMA and GCMMA, versions September 2007. http://www.math.kth.se/~krille/gcmma07.pdf. Accessed 1 November 2010

Taguchi G (1984) Quality engineering through design optimization. Kraus International Publications, New York

Takezawa A, Nii S, Kitamura M, Kogiso N (2011) Topology optimization for worst load conditions based on the eigenvalue analysis of an aggregated linear system. Comput Methods Appl Mech Eng 200(25–28):2268–2281

Yonekura K, Kanno Y (2010) Global optimization of robust truss topology via mixed integer semidefinite programming. Optim Eng 11(3):355–379

Zaman K, McDonald M, Mahadevan S, Green L (2011) Robustness-based design optimization under data uncertainty. Struct Multidisc Optim 44(2):183–197

Zhao ZH, Han X, Jiang C, Zhou XX (2010) A nonlinear interval-based optimization method with local-densifying approximation technique. Struct Multidisc Optim 42(4):559–573